Control and Enhancement of the Oxygen Storage Capacity of Ceria Films by Variation of the Deposition Gas Atmosphere During Pulsed DC Magnetron Sputtering

Asmaa Eltayeb[a,1], Rajani K. Vijayaraghavan[a], Anthony McCoy[b], Anita. Venkatanarayanan[d], Aleksey A. Yaremchenko[e], Rajesh Surendran[e], Stephen Daniels[a], Enda McGlynn[c]

[a] *National Centre for Plasma Science and Technology, School of Electronic Engineering, Dublin City University, Glasnevin, Dublin 9, Ireland*

[b] *School of Physical Science, Dublin City University, Glasnevin, Dublin 9, Ireland*

[c] *School of Physical Science, National Centre for Plasma Science and Technology, Dublin City University, Glasnevin, Dublin 9, Ireland*

[d] *Biomedical Diagnostics Institute, National Center for Sensor Research, School of Chemical Sciences, Dublin City University, Dublin 9, Ireland*

[e] *Department of Materials and Ceramic Engineering, CICECO, University of Aveiro, 3810-193 Aveiro, Portugal*

Abstract

In this study, nanostructured ceria (CeO_2) films are deposited on Si(100) and ITO coated glass substrates by pulsed DC magnetron sputtering using a CeO_2 target. The influence on the films of using various gas ambients, such as a high purity Ar and a gas mixture of high purity Ar and O_2, in the sputtering chamber during deposition are studied. The film compositions are studied using XPS and SIMS. These spectra show a phase transition from cubic CeO_2 to hexagonal Ce_2O_3 due to the sputtering process. This is related to the transformation of Ce^{4+} to Ce^{3+} and

[1] Corresponding author's email: asmaa.eltayeb2@mail.dcu.ie, Tel: + 353 1 700 7625, Fax: + 353 1 700 5508

indicates a chemically reduced state of CeO_2 due to the formation of oxygen vacancies. TGA and electrochemical cyclic voltammetry (CV) studies show that films deposited in an Ar atmosphere have a higher oxygen storage capacity (OSC) compared to films deposited in the presence of O_2. CV results specifically show a linear variation with scan rate of the anodic peak currents for both films and the double layer capacitance values for films deposited in Ar/O_2 mixed and Ar atmosphere are $(1.6 \pm 0.2) \times 10^{-4}$(1.6 ± 0.2) x 10^{-4} F and$(4.3 \pm 0.5) \times 10^{-4}$ (4.3 ± 0.5) x 10^{-4} F, respectively. Also, TGA data shows that Ar sputtered samples have a tendency to greater oxygen losses upon reduction compared to the films sputtered in an Ar/O_2 mixed atmosphere.

Keywords: CeO_2; Oxygen storage capability; Magnetron sputtering; Thin films; Cyclic voltammetry; TGA.

1. Introduction

Research on the nanoscale properties of CeO_2 and CeO_2-based materials, in particular for their oxygen storage capacity (OSC), remains a widespread and popular theme. This is due to the fact that CeO_2 can oxidise and reduce molecules which interact with its surfaces and thus oxygen vacancy defects (OVDs) can be rapidly formed and eliminated, giving CeO_2 its high OSC [1]. This capacity makes various modern devices containing CeO_2 much more effective than their predecessors without CeO_2. The presence of CeO_2 contributes significantly to the effectiveness of three-way catalysts [2], catalysts for H_2 production from fuel [3], optical films [4], oxygen sensors [5] and thermochemical two-step water-splitting cycle [6]. Apart from the ability of CeO_2 to easily and repeatedly switch between oxidation states and accommodate different levels of surface and bulk oxygen vacancies [7], the

abundance of metallic Ce on earth makes CeO_2 a low-cost and highly attractive material for applications in solar cells and photocatalysis. CeO_2 has a cubic fluorite-type crystal structure, with a lattice spacing of 0.5411 nm, and unique material properties such as high dielectric constant, high refractive index and excellent stability at high temperatures [8, 9]. Additionally, CeO_2 is a non-toxic and stable material with a wide band gap. In addition it can demonstrate high ionic conductivity if doped with aliovalent cations [10].

CeO_2 in bulky and porous structures is widely used in many applications relying on the material's enhanced catalytic behaviour and redox properties, as mentioned above. Likewise, thin films can be utilised for the same catalytic applications through the creation of thick porous CeO_2 structures by effectively incorporating porosity between intermediate thin film layers [11, 12], where an understanding and enhancement of the oxygen storage properties of the thin films is essential. Therefore using thin films with higher OSC to create the bulk porous structures would effectively enhance the performance of the final structure. Additionally, and since the physical and chemical properties of CeO_2 can be tuned by doping, these CeO_2 thin films can be doped with materials such as SiO_2, TiO_2 or ZrO_2 in order to improve the thermal stability and oxygen storage (redox) properties of CeO_2 [7].

There are various techniques reported for the preparation of CeO_2 thin films. These include sol-gel deposition [13], e-beam evaporation [14], laser ablation [15], molecular beam epitaxy (MBE) [16], RF magnetron sputtering [17, 18]. Among these techniques, sputtering is one of the best methods for preparation of CeO_2 films due to its many advantages, such as low substrate temperature, good surface roughness characteristics and scalability, as well as being a well-established and relatively low cost industrial technique. The bipolar pulsed DC magnetron sputtering (PDCMS) process has recently attracted a great deal of attention because it shows higher deposition rates of defect-free ceramic films than the more conventional RF magnetron sputtering process. It can in particular alleviate the occurrence of

arcing events at the oxide targets involved in the continuous DC sputtering process, and therefore creating pulses in the magnetron discharge in the mid-frequency range has been found to prevent arc events and stabilize the reactive sputtering process. Thus, PDCMS is a commercially suitable method for large-area deposition of good quality ceramic films with high yield under various processing conditions.

Many reports have addressed the electrochemical, redox and oxygen storage properties of CeO_2 [19-21]. For example, Wang *et al.* [22] introduced a simple OSC measurement technique using cyclic thermogravimetric analysis where the mass changes of the CeO_2 samples, using extra low-temperature, are measured and correlated to OSC. Other groups have also reported on the electrochemical properties and charge storage of CeO_2 such as Brezesinski *et al.*'s report [11] on enhancement in the electrochemical charge storage capacity of the mesoporous ceria compared to bulk ceria and on the oxidation state of Ce in CeO_2 using XPS [19, 23, 24]. Park *et al.* [25] reported the first studies of CeO_2 films deposited by pulsed DC magnetron sputtering where comparative studies of the microstructure and mechanical properties of deposited films were carried out. This work focusses on CeO_2 films deposited on Si(100) and ITO coated glass substrates by PDCMS technique in both a high purity Ar atmosphere and an Ar/O_2 mixed atmosphere. The morphology, electrochemical and voltammetric properties of the CeO_2 films were investigated using AFM, XPS, CV and TGA. The key new outcome from this work is to demonstrate that the OSC of CeO_2 thin films can be controlled and enhanced by varying the gas atmosphere during deposition.

2. Materials and Experimental Section

2.1 Films preparations

CeO_2 films were prepared on Si(100) and ITO coated glass substrates by a magnetron

sputtering system fitted with a CeO_2 target (99.99% purity, Kurt J. Lesker Company) and a pulsed DC power supply (ENI RPG-100 pulse generator) in the power regulation mode. Prior to growth, the substrates were cleaned using acetone and decontamination foam followed by deionised water to remove surface impurities. The chamber was first pumped down to a base pressure of 2×10^{-5} Pa by cryogenic pumping. The target was then pre-sputtered for 10 minutes to eliminate target surface contamination and to obtain a stable plasma density. Sputtering was then performed under both pure argon (Ar) ambient and argon/oxygen (Ar/O_2) mixed ambient and the working pressure was adjusted and kept at 0.7 Pa for the duration of deposition in both cases. The $Ar:O_2$ partial pressure ratio in the Ar/O_2 mixed ambient was 2:1. The sputtering was completed with a power of 65W at 150 kHz without intentional heating using a target to substrate distance of 60 mm. The substrates were held at floating potential and the sputtering time was adjusted to 60 minutes to obtain a uniform film thickness of 50 ± 10 nm for all the samples grown (measured with a J. A. Woollam Co., Inc. M-2000UI Ellipsometer).

2.2 Characterisation techniques

2.2.1 AFM

The surface morphology and roughness of the CeO_2 films were investigated using a Veeco Nanoscope Dimension 3100 atomic force microscope (AFM) instrument operating in tapping mode using aluminium-coated silicon (Si) AFM probes (purchased from Budget Sensors Ltd.). These probes operate at a resonant frequency of 30 kHz and have a force constant of 40 N/m. All AFM images have been measured with the same type of tip in order to ensure the comparability of the determined values of surface roughness (R_{rms}). The R_{rms} values have been calculated using NanoScope Analysis software from 2 μm × 2 μm AFM images.

2.2.2 SIMS and XPS

Secondary ion mass spectrometry (SIMS) and X-ray photoelectron spectroscopy (XPS) and were performed *ex-situ* in two different analysis chambers. SIMS studies were carried out using a quadrupole apparatus (MiniSIMS developed by Millbrook Instruments Ltd). This instrument incorporates a raster scanned gallium liquid metal ion gun for the primary beam and low-energy optics for secondary ion extraction into a 300Da quadrupole. Ga^+ ions (6 keV) were focussed and directed on to the substrate at normal incidence. The SIMS chamber operating pressure was 3.1×10^{-5} Pa.

XPS analysis was carried out using a VG Microtech electron spectrometer with a base pressure of 1×10^{-7} Pa. The photoelectrons were excited with a conventional Mg K_α ($h\nu$ = 1253.6 eV) X-ray source and an electron energy analyser operating at a 20 eV pass energy, yielding an overall resolution of 1.2 eV. The samples were subjected to a mild annealing treatment in UHV at 300 ^oC in order to eliminate any surface contamination, which may have arisen as a result of the transfer in atmosphere between the deposition and analysis chambers.

2.2.3 Electrochemical Measurements – Cyclic Voltammetry (CV)

Electrochemical measurements were conducted using a CH Instruments 660 potentiostat in anhydrous N,N-Dimethylformamide (DMF) solution with 1 M $LiClO_4$ as supporting electrolyte unless otherwise stated. A typical three-electrode cell configuration was used with CeO_2 coated ITO glass as a working electrode and two platinum electrodes, one acting as a counter and the other as a pseudo reference electrode. The active area of the working electrode was maintained constant at 1.44 cm^2 (1.2 cm × 1.2 cm). All potentials have been standardized and quoted versus SCE reference electrode. All chemical and solvents used for electrochemical measurements were purchased from Sigma-Aldrich and were of analytical grade. All solutions were deoxygenated for 30 minutes using nitrogen gas prior to use. All measurements were carried out at room temperature, 22 ± 2 °C.

2.2.4 Thermogravimetric analysis (TGA)

Thermogravimetric analysis (TGA) was performed using a Setaram SetSys 16/18 instrument (sensitivity 0.4 µg). Each TGA sample consisted of several prices of CeO_2 film-covered substrate placed in an alumina crucible. The initial total weight of the samples was 140 mg - 210 mg. The experimental procedure included heating the sample in air to 600 °C, equilibration at this temperature with air for 3 h, flushing with Ar for 1 h, and then reduction in a flow of 10% H_2-N_2 gas mixture for 5 h. The TGA data were corrected for buoyancy effects by subtracting a baseline recorded under identical conditions using an inert alumina reference sample. The oxygen partial pressure in a 10% H_2-N_2 gas mixture at 600 °C corresponded to ~ 10^{-21} Pa.

3. Result and discussion

3.1 Morphological Studies - AFM

The surface morphologies of the CeO_2 sputtered films are shown in Fig. 1. The RMS surface roughness (R_{rms}) of the films were measured from the AFM images and an increase in the R_{rms} of the films from 0.06 nm to 0.19 nm has been observed for the Ar and Ar/O_2 sputtered samples, respectively. Films sputtered in pure Ar show a very smooth, rather featureless, surface structure whereas the films sputtered in an Ar/O_2 mixture show evidence of a slightly rougher surface, as well as some isolated larger grains. These isolated grain features, of different sizes, are observed throughout the Ar/O_2 samples and are possibly due to the formation of polycrystalline CeO_2 as a result of introducing oxygen in the plasma. Suchea *et al*. [26] reported that the introduction of oxygen in the plasma is generally believed to support the formation of grains in metal-oxide films due to the impact/presence of high-energy neutral oxygen atoms [26], [27].

3.2 SIMS

Fig. 2 shows the SIMS spectra of CeO_2 sputtered films, grown in Ar and Ar/O_2, respectively, for the mass region from 110 to 200 amu, where the most intense secondary ion peaks can be seen (CeO^+ for Ar and CeO_2^+ for Ar/O_2 samples). Various oxidation states of the cerium ion and cerium-oxygen molecular ions can be seen, including CeO^+, CeO_2^+, Ce_2O^+, $Ce_2O_2^+$ and $Ce_2O_3^+$ ions. The typical secondary ions seen in CeO_x mixed oxide spectra are summarised in Table 1 together with corresponding m/q values [28]. In case of CeO^+ and $CeOH^+$, there is mass interference/overlapping hence multiple peaks are detected between 155.4 amu and 157.9 amu with a higher $CeOH^+$ intensity observed for the Ar/O_2 sputtered sample.

3.3 XPS

The CeO_2 film surface compositions have been studied by XPS to probe the presence of Ce in the Ce^{4+} and Ce^{3+} charge states in the material. In particular, CeO_2 films in a chemically reduced state should show XPS peaks corresponding to the Ce^{3+} state [29] and CeO_2 films should show XPS peaks corresponding to the Ce^{4+} state. XPS scans show the Ce3d peaks (Fig. 3) and characteristic O1s (Fig. 4) and, from which the film stoichiometry and bonding type can be determined. Fig. 3 displays the core Ce3d levels of the two CeO_2 sputtered films, in Ar and Ar/O_2 atmospheres. The XPS spectrum from the CeO_2 is complex and split into $Ce3d_{3/2}$ and $Ce3d_{5/2}$ peaks, due to spin-orbit coupling effects. The peaks in the region 875-895 eV correspond to the $Ce3d_{5/2}$ while peaks in the region 895-910 eV correspond to the $Ce3d_{3/2}$ levels [19, 30]. The characteristic peak energies associated with different Ce charge states are indicated by the vertical dotted lines. The spectra clearly show the greater concentration of Ce in the Ce^{3+} oxidation state in the sample grown in Ar, indicating a chemically reduced state of CeO_2. This greater concentration of the Ce^{3+} oxidation state the sample grown in Ar is easily seen by virtue of the peaks at $881.2 \pm \pm 0.5$,

886.5 ± ±0.3, 901.2 ± ±0.5 and 904.5 ± ±0.3 eV [23]. The Ce^{3+}/Ce^{4+} ratio of CeO_2 samples sputtered in Ar and Ar/O_2 are 4.29 and 1.92, respectively. These values are calculated by comparing the integrated area of the fitted Ce^{3+} and Ce^{4+} peaks.

Fig. 4 shows an O 1s spectrum fitted with two Voigt functions. The main component labelled 'i' has a binding energy of 529.4 eV and is due to O^{2-} ions [24]. At the high-binding-energy side there is an additional peak labelled 'ii'. Based on our fitting, the binding energy is 531.1 eV, but the exact value is difficult to determine. This is because the peaks are rather broad and feature 'ii' is not very pronounced the formation of $O^{\delta-}$ species and thus, the presence of OH groups or carbon contamination at the surface have been discussed as possible explanations for this component [19, 24].

3.4 Electrochemistry –CV

It is widely known that oxygen vacancies contribute to and enhance the charge storage capacitance of metal-oxides such as MnO_2 [31], ZnO [32], SiO_2 [33] and TiO_2 [34]. It is also known that ceria is a suitable material for charge storage due to the ability of Ce to cycle between Ce^{4+}/Ce^{3+} redox states [11, 35]. Therefore, oxygen vacancies can be correlated directly to the charge storage capacity (CSC) since these may act as charge carriers [34]. Here, CV measurements of the sputtered CeO_2 films (shown in Fig. 5) were recorded at various scan rates ranging from 10 to 800 mVs^{-1}. This was done to examine the redox process present in DC sputtered CeO_2 thin films and to determine the CSC of the films. Fig. 5 shows CV curves of the sputtered CeO_2 films grown in Ar and Ar/O_2 gas atmospheres in 1 M $LiClO_4$. CeO_2 films sputtered in Ar display two peaks at 0.5 V and 1.2 V where partial oxidation of CeO_2 may occur. These peaks only appear on the CeO_2 films sputtered in Ar as opposed to CeO_2 films sputtered in Ar/O_2. The negative currents observed during the negative scan suggest a reduction process, probably reduction of oxygen ions [21]. Equation

1 is used to determine the double layer capacitance, i.e. the CSC of the films for different scan rates.

$$i = vC_{dl} \quad (1)$$

where, i is the charging current, v is the scan rate and C_{dl} is the electrochemical double layer capacitance [36].

The current is measured at -0.1 V for the CeO_2 films sputtered in Ar/O_2 and at -0.2 V for the CeO_2 films sputtered in Ar in order to avoid inclusion of any Faradaic current or pseudo capacitance effects. Significantly, the peak anodic currents (capacitive current, i_a) for both the films varied linearly with scan rate as shown in Fig. 6, with double layer capacitance (C_{dl}) values of $(1.6 \pm 0.2) \times 10^{-4}$ F for the CeO_2 films sputtered in Ar/O_2 and $(4.3 \pm 0.5) \times 10^{-4}$ F for the CeO_2 films sputtered in Ar, respectively. These values show that there is a more than two fold increase in the CSC when the film is deposited in Ar compared to the sample deposited in the presence of O_2. The reason for this increase in CSC is thought to be due to absence of oxygen atoms within the deposition chamber, which in consequence does not aid oxygen diffusion process through the lattices. It is important to note that the active surface area of both the films is maintained constant at 1.44 cm^2. Thus, these results demonstrate that CeO_2 films grown using a pure Ar sputtering ambient significantly enhances the electrochemical charge storage properties.

3.5 OSC measurements - TGA

Typical OSC measurements require relatively complicated experimental setups. These methods involve gas-phase reactions in pulse mode (flow titration, and gas chromatography or mass spectrometry for detection) [37, 38]. Therefore, a simple OSC measurement technique introduced by *Wang et al.* [22] is used in this work, where the mass changes of the CeO_2 samples are measured and correlated to OSC using cyclic TGA. Here we used a single TGA cycle to assess the mass change of supported CeO_2 sample on reduction. After 5 h of

reduction at 600°C, the overall mass change for Ar/O_2 - CeO_2 sample was below the detection limit, i.e. < 0.01 mg which corresponds to experimental uncertainty (due to natural baseline drifts). By contrast, the Ar - CeO_2 sample, under similar conditions, demonstrated a detectable mass loss of ~ 0.024 mg which corresponds to approximately 0.017% of the total sample mass or to ~ 4.7% of theoretical mass of the nanostructured CeO_2 thin film. We note that the equilibrium oxygen nonstoichiometry (δ) in the bulk microcrystalline $CeO_{2-\delta}$ under similar conditions (600°C and $p(O_2) \sim 10^{-21}$ Pa) is reported to be as low as ~ 0.01 [39]. Very small nonstoichiometry variations at this temperature make it impossible to determine the OSC of thin films with higher precision. Nevertheless, the results of our thermogravimetric studies clearly show that the samples sputtered in argon atmosphere have a tendency to greater oxygen losses (and therefore higher OSC) upon reduction in a 10 % H_2 flow at 600 °C compared to the films sputtered in Ar/O_2 mixed atmosphere.

4. Conclusion

In this study, a reliable method for the deposition of stable CeO_2 thin films using pulsed DC magnetron sputtering has been successfully demonstrated. A uniform film thickness of 50 $\pm$10 nm was obtained for all the deposited samples. The effect of two sputtering gas ambient on the morphological, electrochemical and oxygen storage properties have been studied, and the following key conclusions are reached on the basis of our results. Firstly, the deposition gas ambient influenced the surface morphology of CeO_2 films. Secondly, the relative oxygen deficiency in the sample sputtered in Ar has been confirmed by AFM, SIMS, XPS, CV and TGA. Finally, the electrochemical measurements and TGA analysis both indicate that CeO_2 samples sputtered in Ar have a higher CSC and OSC than those deposited in the presence of O_2, making CeO_2 samples sputtered in Ar better suited for many applications based on the material's enhanced catalytic behaviour and redox properties.

Acknowledgements

A. Eltayeb, S. Daniels and E. McGlynn specifically gratefully acknowledge postgraduate funding from INSPIRE, supported under the framework of the Irish government's PRTLI cycle 5, national development plan 2007-2013 with the assistance of the European regional development fund. S. Daniels and K.V. Rajani also gratefully acknowledge SFI′s Strategic Research Cluster Programme ("Precision" 08/SRC/I1411) for financial support.

References

[1] M. Roeb, M. Neises, N. Monnerie, F. Call, H. Simon, C. Sattler, M. Schmücker, R. Pitz-Paal, Materials, 5 (2012) 2015-2054.

[2] C. Descorme, R. Taha, N. Mouaddib-Moral, D. Duprez, Applied Catalysis A: General, 223 (2002) 287-299.

[3] B. Zhang, X. Tang, Y. Li, Y. Xu, W. Shen, International Journal of Hydrogen Energy, 32 (2007) 2367-2373.

[4] N. Özer, Solar Energy Materials and Solar Cells, 68 (2001) 391-400.

[5] P. Jasinski, T. Suzuki, H.U. Anderson, Sensors and Actuators B: Chemical, 95 (2003) 73-77.

[6] W.C. Chueh, C. Falter, M. Abbott, D. Scipio, P. Furler, S.M. Haile, A. Steinfeld, Science, 330 (2010) 1797-1801.

[7] B.M. Reddy, A. Khan, Catalysis Surveys from Asia, 9 (2005) 155-171.

[8] J. Owens, E. Tarte, P. Berghuis, R. Somekh, Applied Superconductivity, IEEE Transactions on, 5 (1995) 1657-1660.

[9] N. Savvides, A. Thorley, S. Gnanarajan, A. Katsaros, Thin Solid Films, 388 (2001) 177-182.

[10] H. Yahiro, Y. Eguchi, K. Eguchi, H. Arai, Journal of Applied Electrochemistry, 18 (1988) 527-531.

[11] T. Brezesinski, J. Wang, R. Senter, K. Brezesinski, B. Dunn, S.H. Tolbert, ACS nano, 4 (2010) 967-977.

[12] S.G. Rudisill, L.J. Venstrom, N.D. Petkovich, T. Quan, N. Hein, D.B. Boman, J.H. Davidson, A. Stein, The Journal of Physical Chemistry C, 117 (2013) 1692-1700.

[13] P. Periyat, F. Laffir, S. Tofail, E. Magner, RSC Advances, 1 (2011) 1794-1798.

[14] M. Anwar, S. Kumar, F. Ahmed, N. Arshi, Y.J. Seo, C.G. Lee, B.H. Koo, Current Applied Physics, 11 (2011) S301-S304.

[15] H. Nagata, T. Tsukahara, S. Gonda, M. Yoshimoto, H. Koinuma, Japanese journal of applied physics, 30 (1991) L1136.

[16] J. Jones, E. Croke, C. Garland, O. Marsh, T. McGill, Journal of Vacuum Science & Technology B, 16 (1998) 2686-2689.

[17] M.-T. Ta, D. Briand, Y. Guhel, J. Bernard, J. Pesant, B. Boudart, Thin Solid Films, 517 (2008) 450-452.

[18] K. Sundaram, P. Wahid, O. Melendez, Journal of Vacuum Science & Technology A, 15 (1997) 52-56.

[19] D. Mullins, S. Overbury, D. Huntley, Surface Science, 409 (1998) 307-319.

[20] M.Y.M. Abdelrahim, S.R. Benjamin, L.M. Cubillana-Aguilera, I. Naranjo-Rodríguez, J.L. de Cisneros, J.J. Delgado, J.M. Palacios-Santander, Sensors, 13 (2013) 4979-5007.

[21] Q. He, S. Mukerjee, B. Shyam, D. Ramaker, S. Parres-Esclapez, M. Illán-Gómez, A. Bueno-López, Journal of Power Sources, 193 (2009) 408-415.

[22] D. Wang, Y. Kang, V. Doan-Nguyen, J. Chen, R. Küngas, N.L. Wieder, K. Bakhmutsky, R.J. Gorte, C.B. Murray, Angewandte Chemie International Edition, 50 (2011) 4378-4381.

[23] L. Garvie, P. Buseck, Journal of Physics and Chemistry of solids, 60 (1999) 1943-1947.

[24] H. Borchert, Y.V. Frolova, V.V. Kaichev, I.P. Prosvirin, G.M. Alikina, A.I. Lukashevich, V.I. Zaikovskii, E.M. Moroz, S.N. Trukhan, V.P. Ivanov, The Journal of Physical Chemistry B, 109 (2005) 5728-5738.

[25] I.-W. Park, J. Lin, J.J. Moore, M. Khafizov, D. Hurley, M.V. Manuel, T. Allen, Surface and Coatings Technology, 217 (2013) 34-38.

[26] M. Suchea, S. Christoulakis, K. Moschovis, N. Katsarakis, G. Kiriakidis, Thin Solid Films, 515 (2006) 551-554.

[27] L. Damiani, R. Mansano, in: Journal of Physics: Conference Series, IOP Publishing, 2012, pp. 012019.

[28] K. Mašek, M. Václavů, P. Bábor, V. Matolín, Applied Surface Science, 255 (2009) 6656-6660.

[29] A. Migani, K.M. Neyman, F. Illas, S.T. Bromley, The Journal of chemical physics, 131 (2009) 064701-064701.

[30] P. Burroughs, A. Hamnett, A.F. Orchard, G. Thornton, Journal of the Chemical Society, Dalton Transactions, (1976) 1686-1698.

[31] Z. Wang, Z. Li, J. Feng, S. Yan, W. Luo, J. Liu, T. Yu, Z. Zou, Physical Chemistry Chemical Physics, 16 (2014) 8521-8528.

[32] Q. Zhu, C. Xie, H. Li, Q. Yang, Journal of Alloys and Compounds, 585 (2014) 267-276.

[33] N. Van Duy, S. Jung, N.T. Nga, D.N. Son, J. Cho, S. Lee, W. Lee, J. Yi, Materials Science and Engineering: B, 175 (2010) 176-180.

[34] M. Salari, S.H. Aboutalebi, A.T. Chidembo, I.P. Nevirkovets, K. Konstantinov, H.K. Liu, Physical Chemistry Chemical Physics, 14 (2012) 4770-4779.

[35] T. Suzuki, I. Kosacki, H.U. Anderson, P. Colomban, Journal of the American Ceramic Society, 84 (2001) 2007-2014.

[36] V. Birss, W. Mustain, D. Wilkinson, P. Kulesza, K. Ota, Electrode Processes Relevant to Fuel Cell Technology, The Electrochemical Society, New Jersey, USA, 2010.

[37] H.-X. Mai, L.-D. Sun, Y.-W. Zhang, R. Si, W. Feng, H.-P. Zhang, H.-C. Liu, C.-H. Yan, The Journal of Physical Chemistry B, 109 (2005) 24380-24385.

[38] G. Zhou, J. Hanson, R.J. Gorte, Applied Catalysis A: General, 335 (2008) 153-158.

Table1

Table 1. m/q values of different observed CeO_δ ion clusters.

Ion	m/q (amu)
Ce^+	140
CeO^+	156
CeO_2^+	172

Fig. 1. 2 ×2 μm^2 top and 3D view AFM images of CeO_2 thin films sputtered in a) pure Ar and b) an Ar/O_2 gas mixture.

Fig. 2. SIMS spectra in the range from 100 to 200 amu measured from CeO_2 thin films sputtered in a) Ar and b) Ar/O_2.

Fig. 3. Ce 3d core level photoemission spectra from CeO_2 thin films sputtered in a) Ar and b) Ar/O_2 gas atmospheres.

Fig. 4. O 1s core level photoemission spectra from CeO_2 thin films sputtered in a) Ar and b) Ar/O_2 gas atmospheres. The component labelled '(i)' is attributed to O^{2-} ions. The component labelled '(ii)' is assigned to $O^{\delta-}$ species or OH groups.

Fig. 5. CV scan of 50 nm thick nanostructured CeO_2 films deposited by pulsed d.c. magnetron sputtering technique in a) a pure Ar environment and in b) an Ar/O_2 mixture environment in anhydrous DMF solution with 1 M LiClO4 as supporting electrolyte and a scan rate of 0.1 Vs^{-1}.

Fig. 6. Relationship between capacitive current (i_a) and scan rate for CeO_2 films deposited in a) pure Ar and b) Ar/O_2 ambients.

Fig. 7. TGA curves of CeO_2 films deposited in a pure Ar ambient and in Ar/O_2 mixed ambient, on reduction in 10%H_2-N_2 flow at 600°C.

Figure_1a_top_view

Click here to download high resolution image

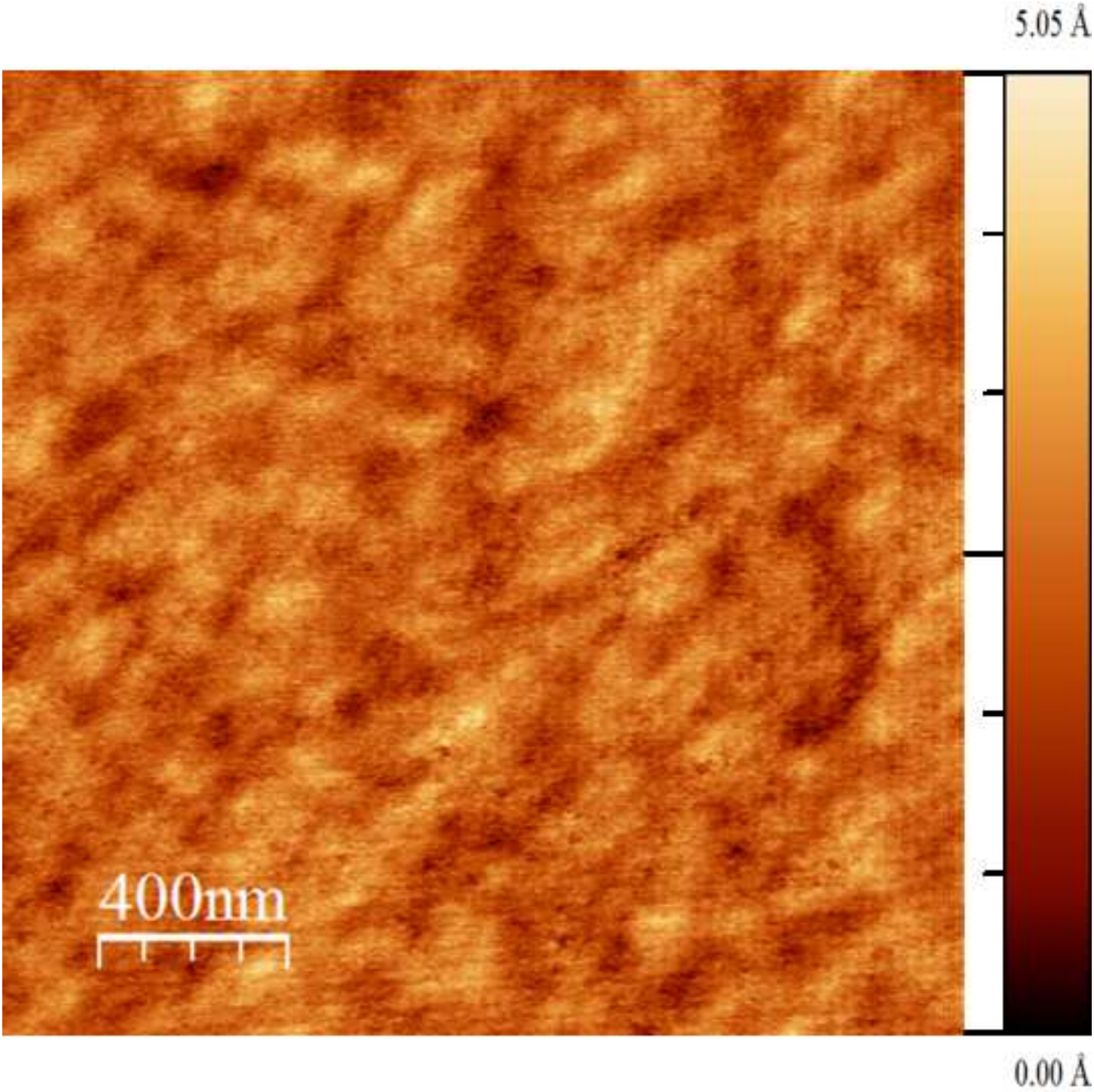

Figure_1a_3D_view

Click here to download high resolution image

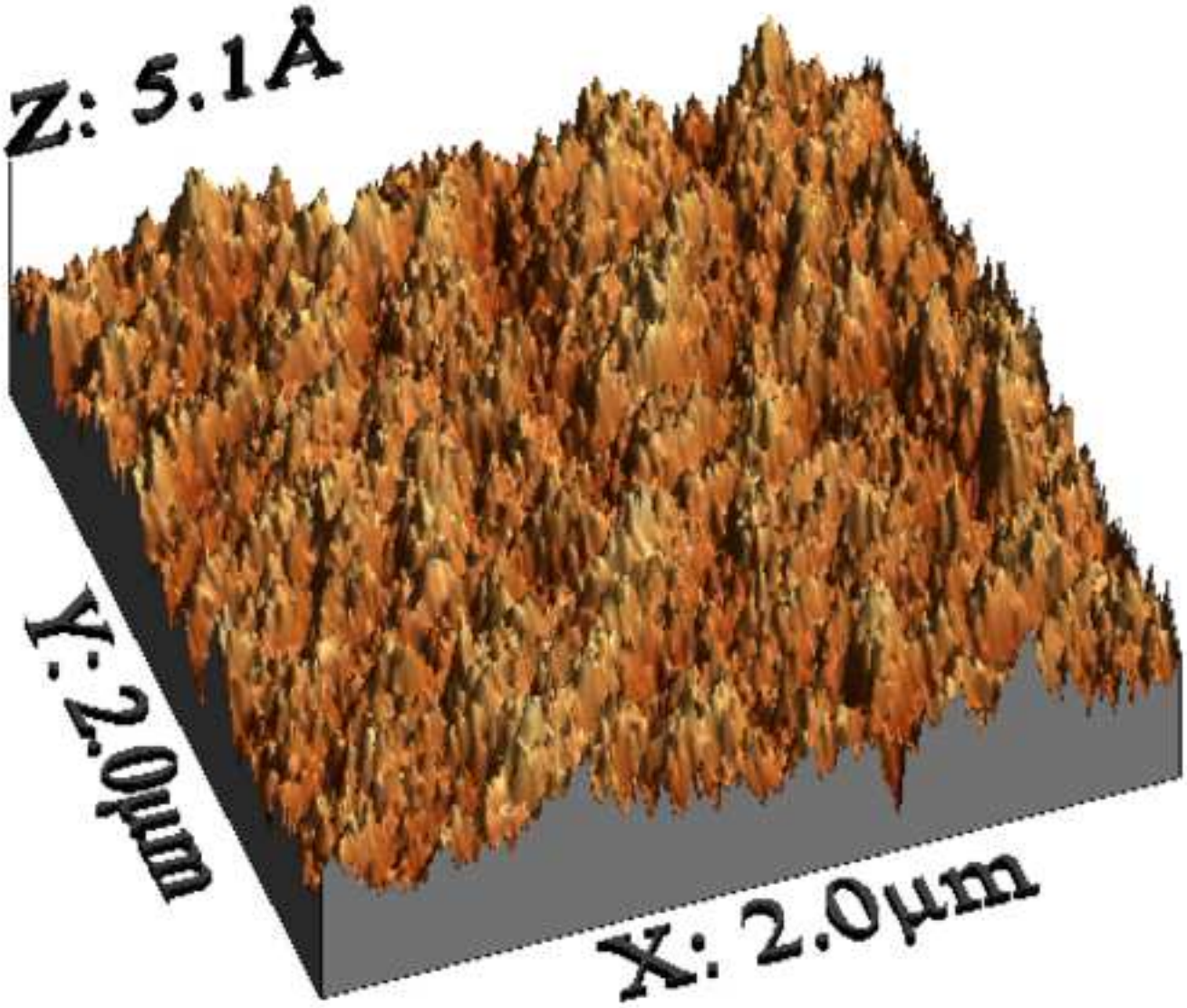

Figure_1b_top_view

Click here to download high resolution image

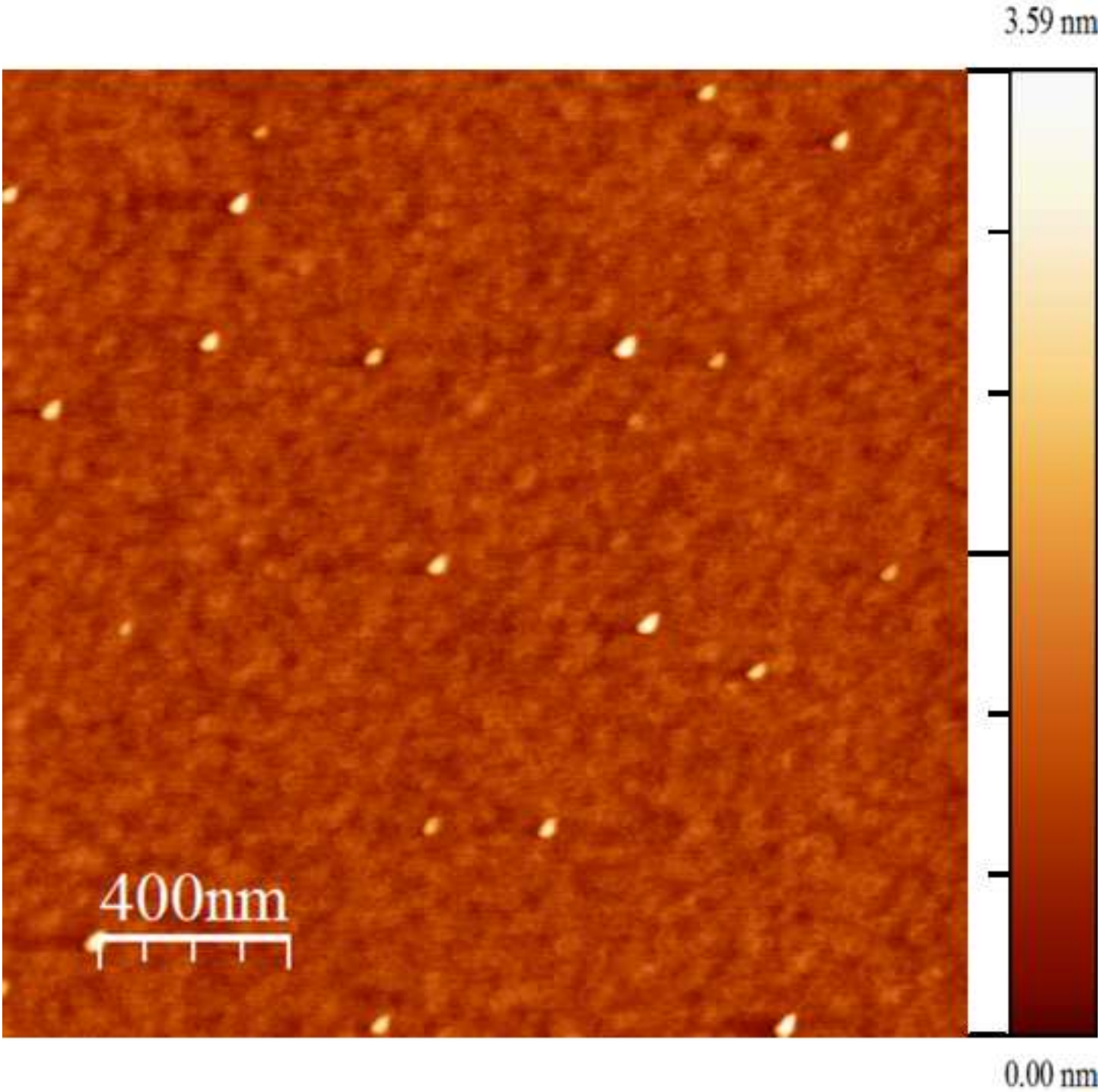

Figure_1b_3D_view

Click here to download high resolution image

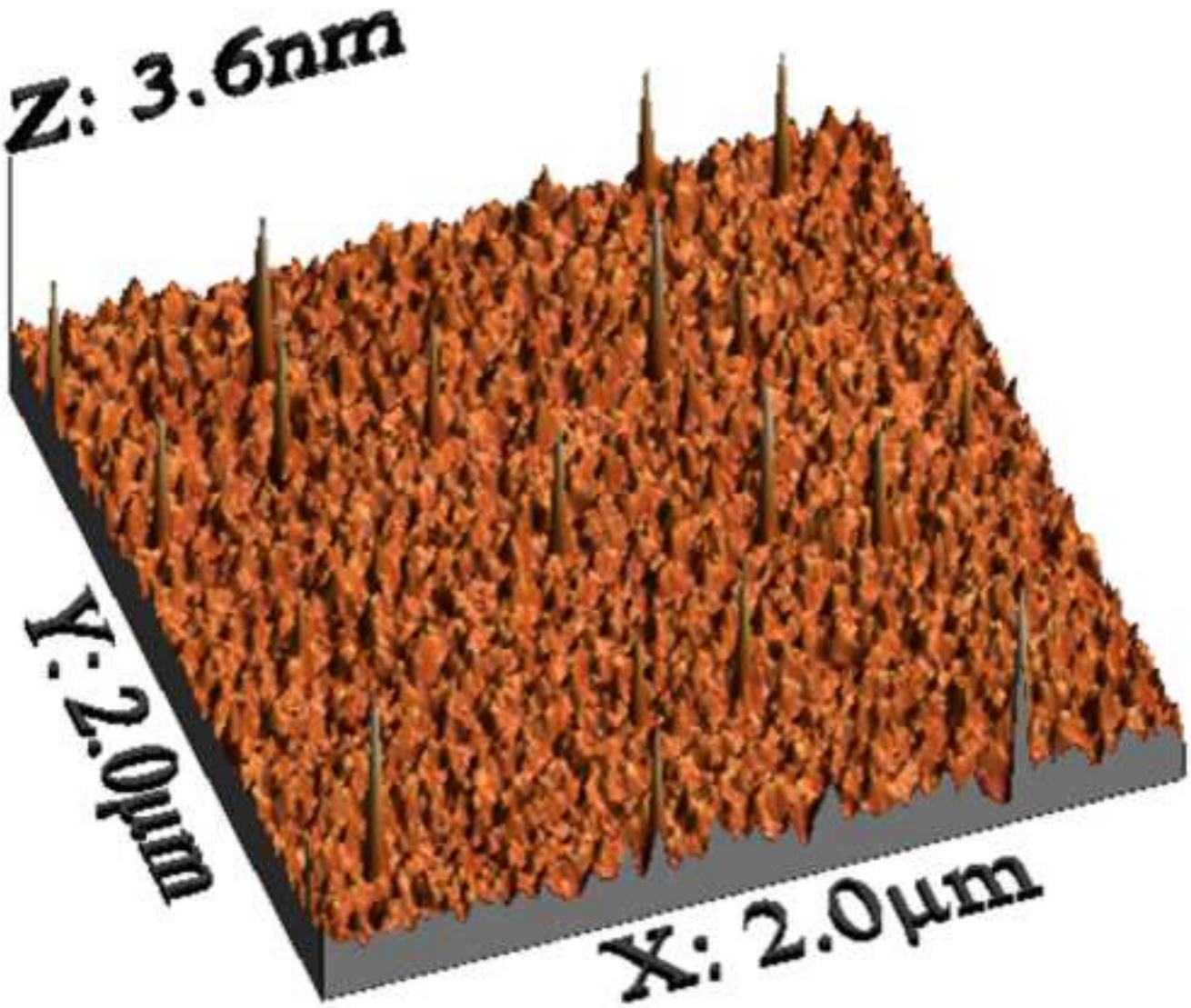

Figure_2a

Click here to download high resolution image

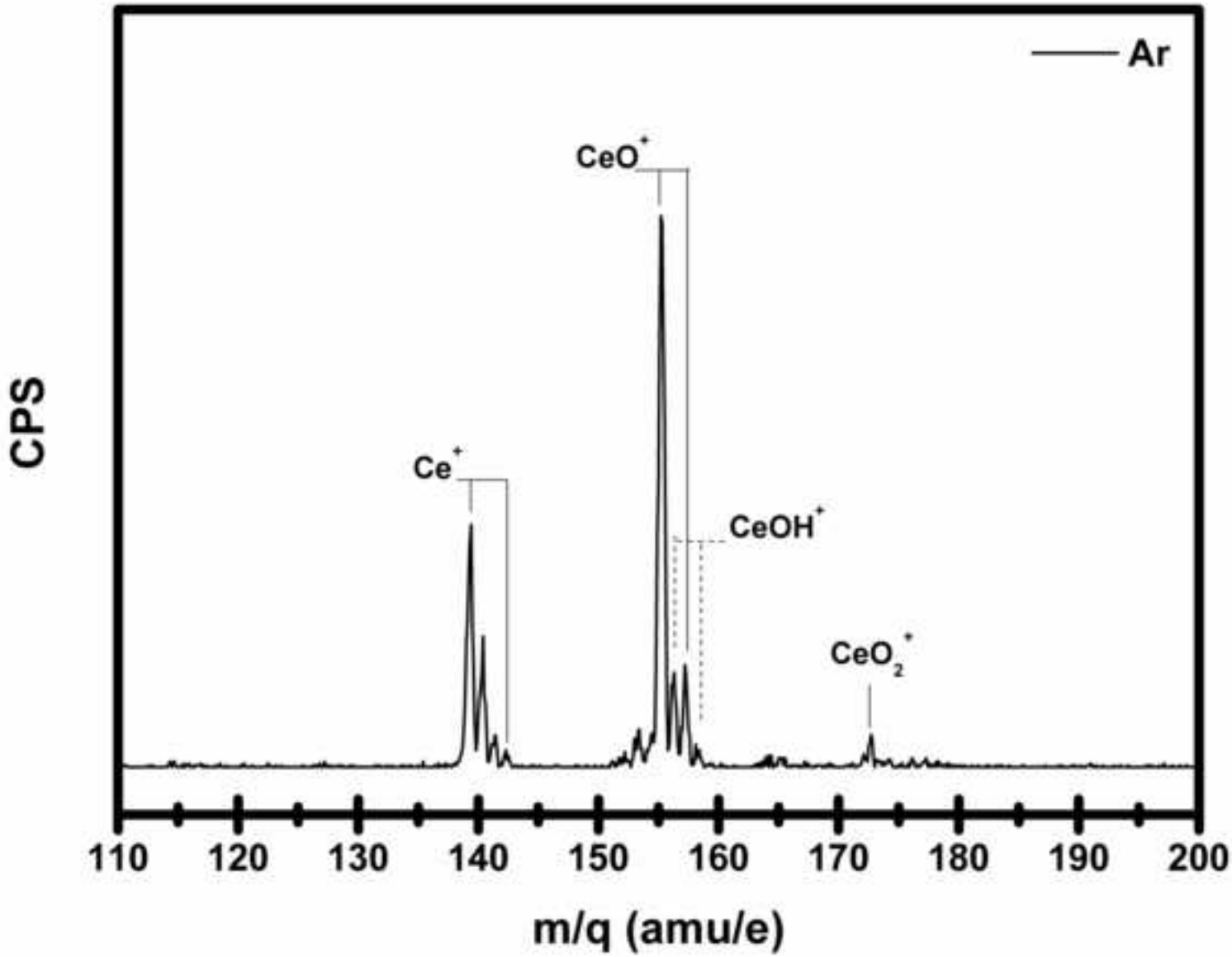

Figure_2b

Click here to download high resolution image

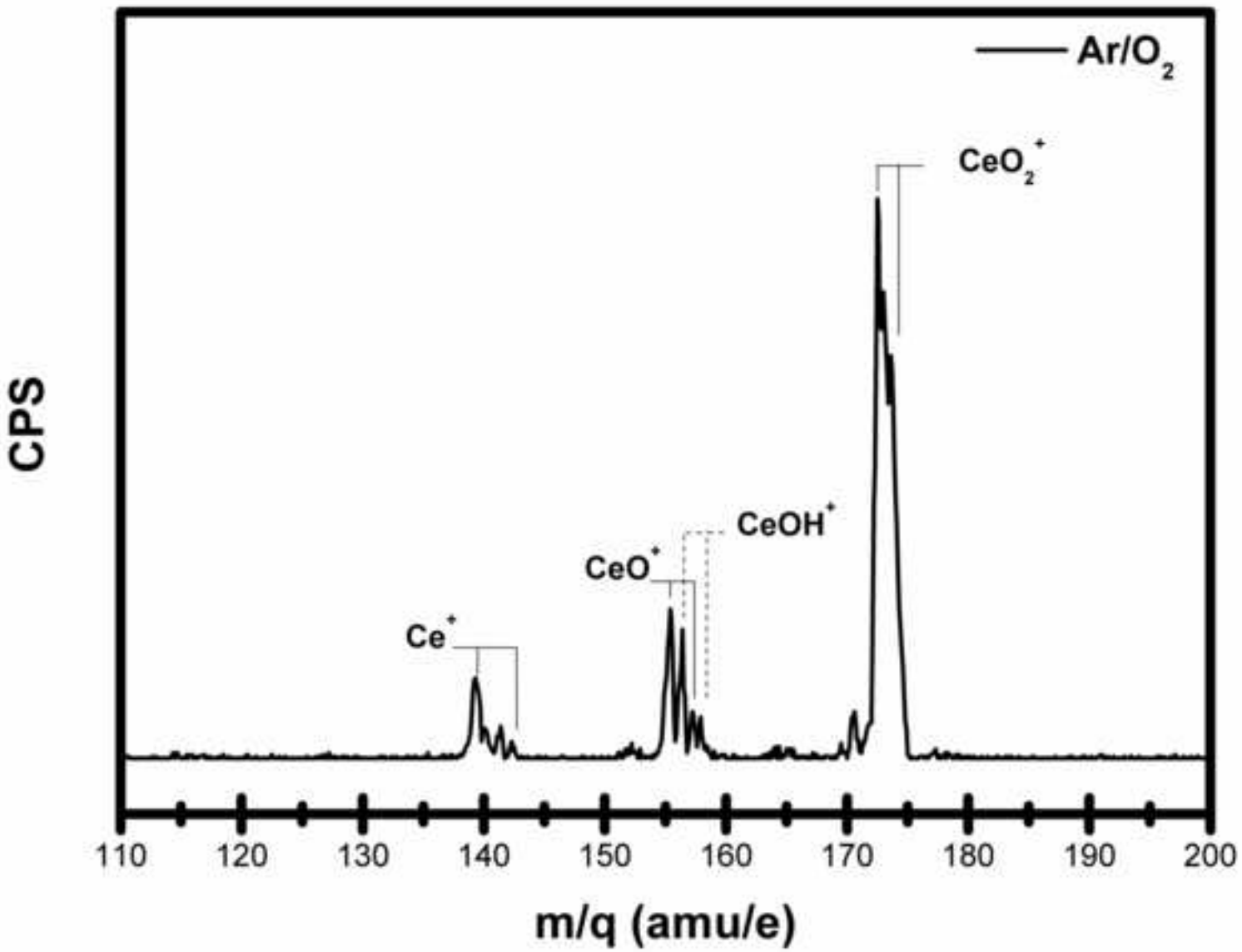

Figure_3
Click here to download high resolution image

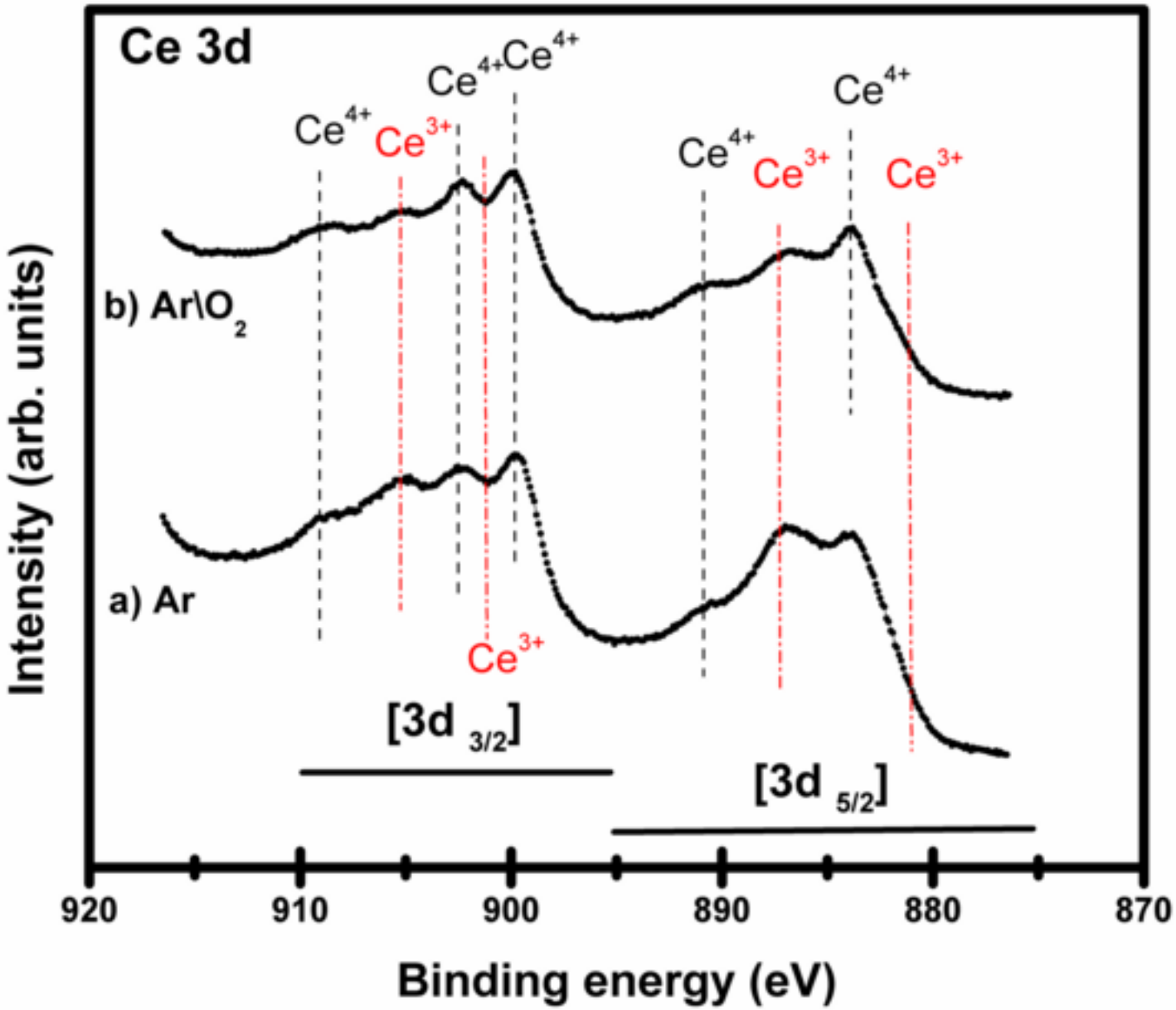

Figure_4
Click here to download high resolution image

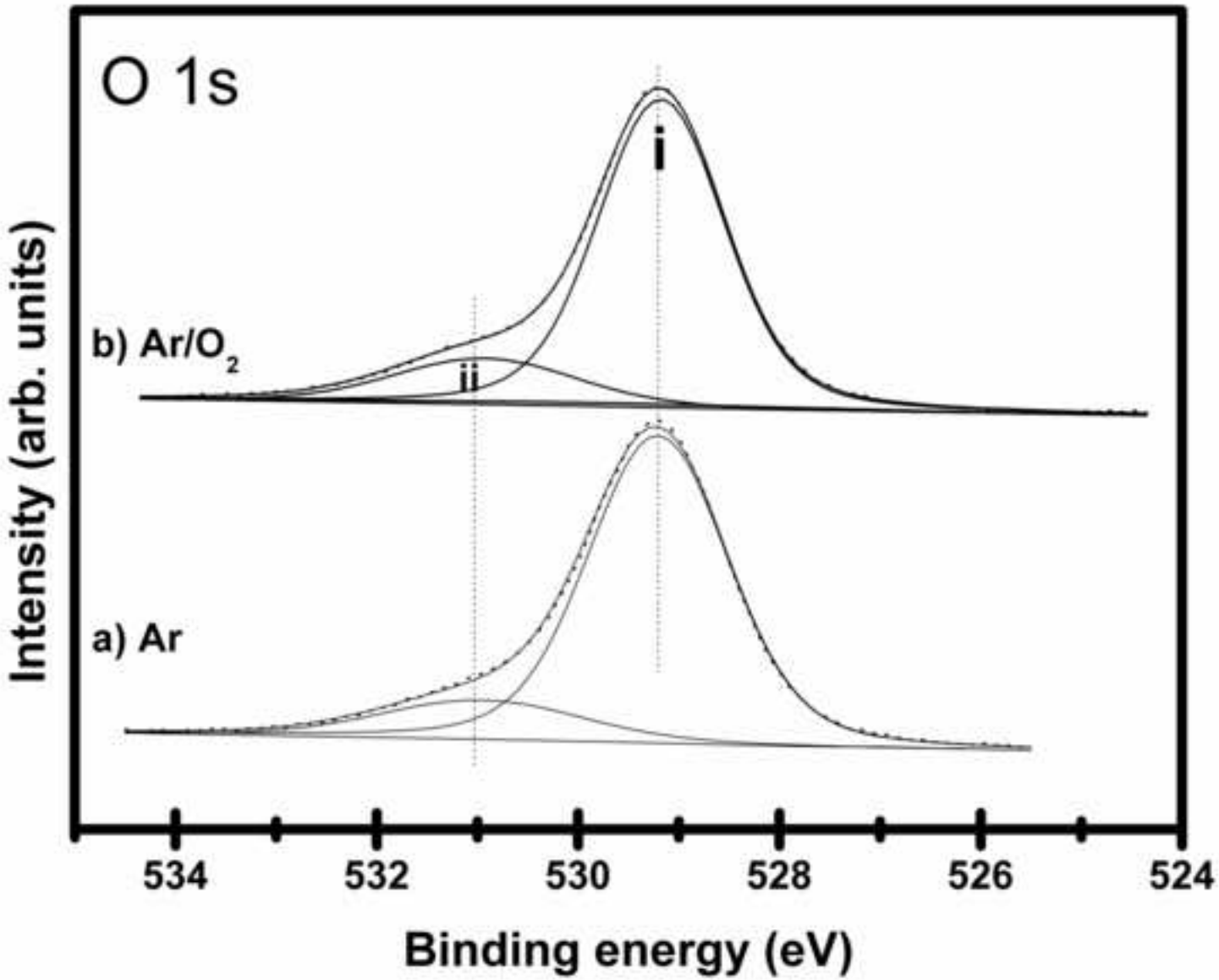

Figure_5
Click here to download high resolution image

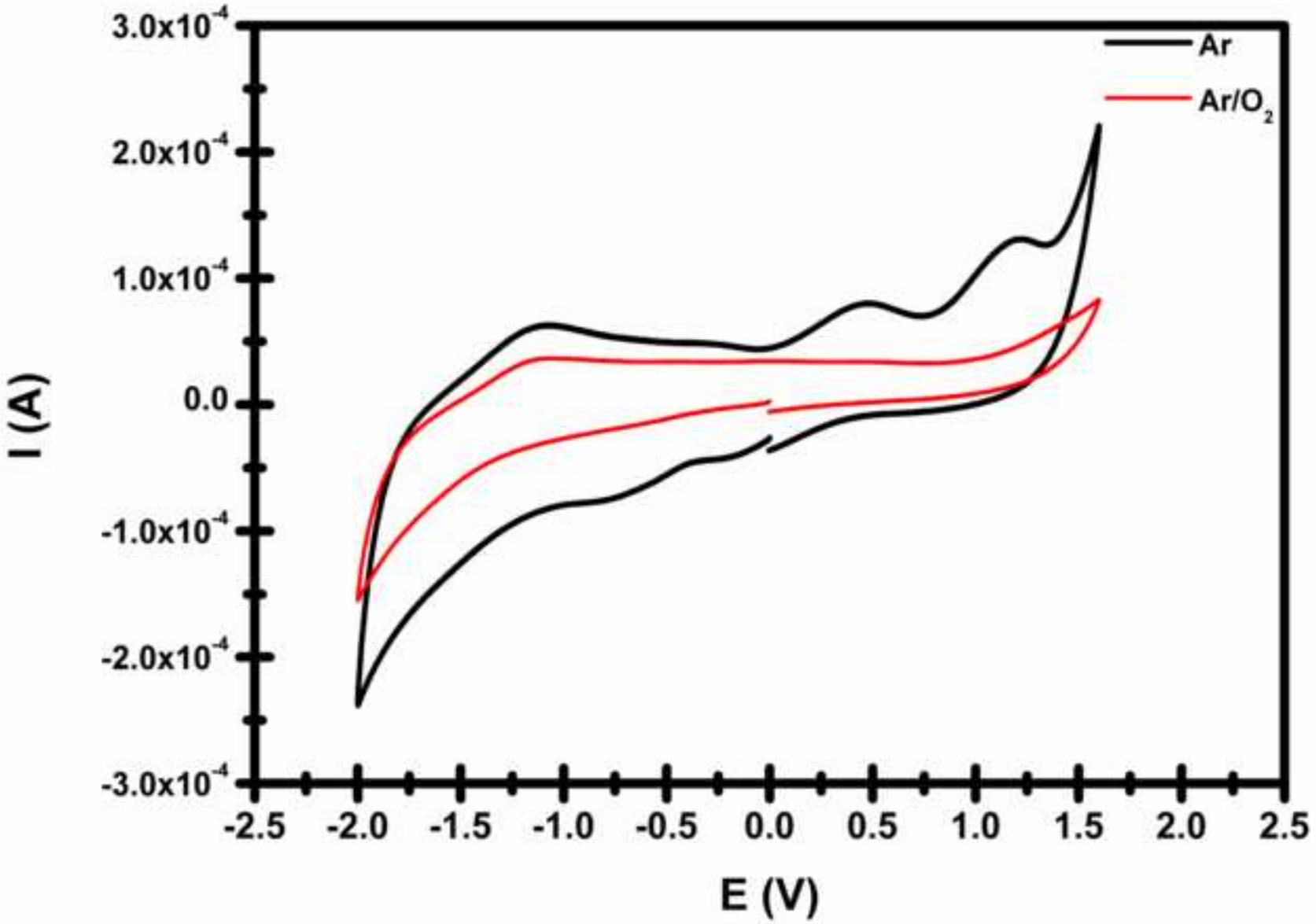

Figure_6
Click here to download high resolution image

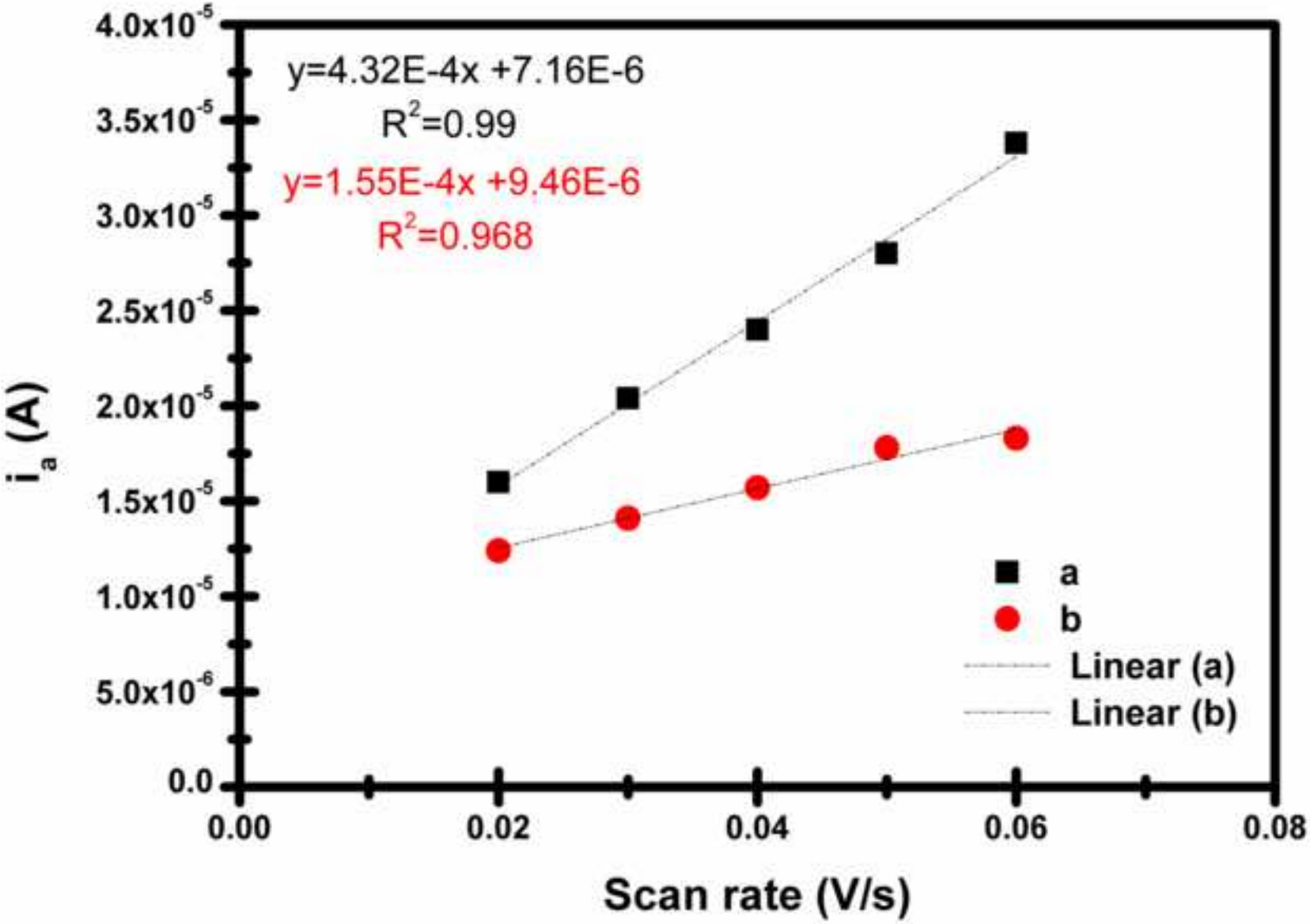

Figure_7
Click here to download high resolution image

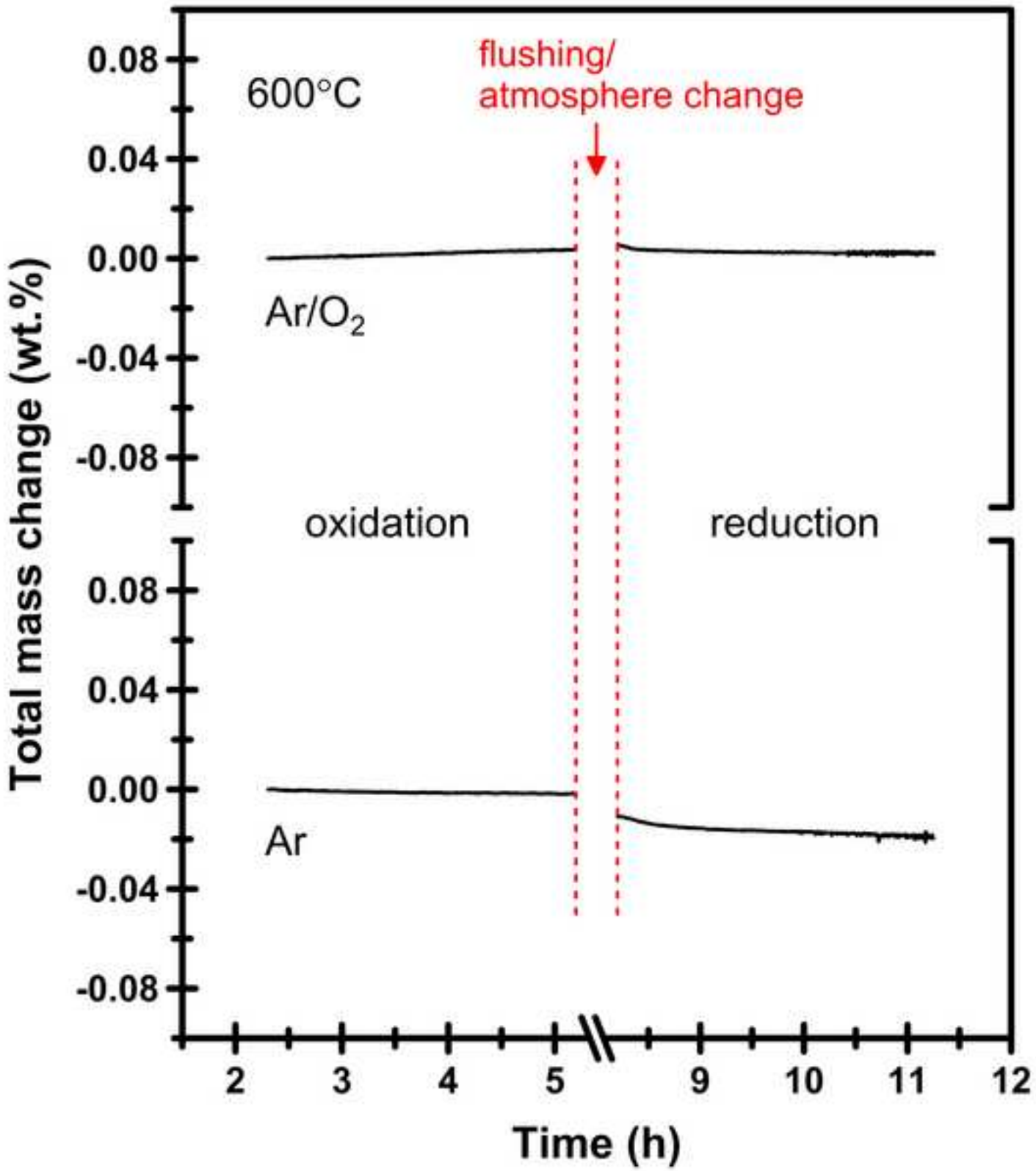

Glossary

Click here to download Supplementary Materials: Glossary.docx